PERGAMON

International Journal of Solids and Structures 38 (2001) 1311–1325

INTERNATIONAL JOURNAL OF SOLIDS and STRUCTURES

www.elsevier.com/locate/ijsolstr

On the effects of the heat generated during an electric field-induced ferroelectric domain switching

Sang-Joo Kim *, Sunggi Kim

Department of Mechanical Engineering, University of Seoul, 90, Chennong-doug, Tongdaemun-gu, Seoul 130-743, South Korea

Received 23 April 1999; in revised form 7 March 2000

Abstract

A ferroelectric material is characterized by its ability of changing the polar direction in the presence of applied electric field. This change of polar direction is called domain switching or polarization reversal. The domain switching occurs in two steps: the nucleation of new domain and the propagation of domain boundary. Recently, "Kim" (Kim, S.J., 2000. Int. J. Solids Struct. 37, 1145–1164) has shown that a certain amount of heat is generated from a moving domain boundary during domain switching. In this paper, we study the effects of the heat generated from a moving domain boundary under an application of electric field. The finite difference algorithm of Kim and Abeyaratne (Kim, S.J., Abeyaratne, R., 1995. Cont. Mech. Thermo 7, 311–333) is applied to the model developed by Kim (2000). The results of calculation are qualitatively consistent with the experimental observation of Hill et al. (Hill, M.D., White, G.S., Hwang C.S., Lloyd I.K., 1996. J. Am. Ceram. Soc. 79, 1915–1920)

Keywords: Ferroelectric domain switching; Moving domain boundary; Heat; Temperature

1. Introduction

One of the characteristics of a ferroelectric material is that it is polarized in the absence of applied electric field at a temperature below the so-called Curie point. This polarization is called spontaneous polarization. An application of electric field may switch the polar direction of the material and this is commonly called polarization reversal or domain switching (Jona and Shirane, 1962). The domain switching occurs in two steps: first, the new domain is nucleated at some critical level of applied electric field, and next, the interface between the two domains propagates leading to the growth of the new domain. As particles cross this moving interface or domain boundary, they transform from one type of domain to the other one, and according to Kim (2000), this is accompanied by the release of heat. This leads to an increase in the temperature near the domain boundary and significantly affects the electrical response of the body. The purpose of the present paper is to investigate this effect of the heat generated from a moving domain boundary during an electric field-induced ferroelectric domain switching.

* Corresponding author. Fax: +11-822-2248-5110.
E-mail address: sjk@uoscc.uos.ac.kr (S.-J. Kim).

0020-7683/01/$ - see front matter
PII: S0020-7683(00)00091-3

Various continuum models for ferroelectric domain switching have been suggested in various scales (e.g., Hwang et al., 1995; Jiang, 1993, 1994; Ghandi and Hagwood, 1996). But none of them studied on the effect of the heat generated during the domain switching process. However, there have been some experimental investigations on this subject. Hill et al. (1996) have applied electrical cyclic-loading on a PZT ceramic and have measured the temperature of the sample. They observed that the temperature of the sample increased up to a steady state temperature of 180°C. The present study has been motivated by this experimental observation.

Recently, Kim (2000) has developed a one-dimensional continuum model for ferroelectric materials. His model consists of three parts: Helmholtz free energy function for each phase of the material, the kinetic relation to control the speed of phase boundary and the nucleation criterion to determine the conditions under which the new phase is nucleated. He showed that there exist two mechanisms by which heat is generated from a moving domain boundary. One is the energy dissipation occurring at the domain boundary, which is represented as the product of the driving force acting on the boundary and the speed of the boundary. The other is from the difference in entropy between the two types of domains across the domain boundary. He considered a very slow electrical loading rate. So, the heat generated at the moving interface diffuse relatively rapidly and the temperature of the body will equilibrate that of the surrounding environment, even as the transformation is still progressing. In this case, the underlying thermoelectrical processes can be modeled as being isothermal, i.e., one can assume that every particle of the body remains at the environmental temperature at every instant of time. Some calculations were carried out based on this isothermal assumption and the results were qualitatively compared with experimental observations in his work.

In the present paper, we consider a somewhat faster electrical loading rate. Then, the temperature field in the body will not be uniform any longer and the domain boundary is regarded as a moving heat source. In order to understand the effect of such local heating, we study the response of a thermopolarizable bar that is contained in a constant environmental temperature and that is subjected to a prescribed electrical loading-history. The model we use consists of a three-well Helmholtz free-energy potential that describes the thermoelectrical behavior of each phase, a kinetic law based on thermal-activation theory which controls the rate of a domain boundary, and a nucleation criterion based on a critical value of energy barriers between phases that signals the initiation of the transformation. The reason we have a three-well energy function is that at low temperatures, the high temperature paraelectric phase is regarded as an unstable phase between the two variants of ferroelectric phase and therefore its value of Gibbs free energy is needed to derive the kinetic relation and nucleation criterion. The main features of our model are as follows. First, the energy equation derived from the model is generally a nonlinear equation and involves coupling between thermal and electrical effects. Similar coupling also exists in the jump condition that represents the energy conservation on the domain boundary. The heat generated at the moving domain boundary is not only due to the energy dissipation at the domain boundary, but also due to the latent heat caused from the difference in specific entropy between the two variants of ferroelectric phase across the boundary. Finally, the domain boundary propagates at a speed that is controlled by the kinetic relation, which depends on the local temperature and electric field.

In Section 2, we outline the general theoretical framework within which the present study is carried out. In Section 3, we describe the particular constitutive model that we use. The basic thermoelectrical responses are formulated in Section 4, and finally, in Section 5, we show and discuss the results of calculations.

2. Theoretical framework

In this section, we set out the basic equations which describe our model. We consider a one-dimensional bar, which occupies the interval $0 \leqslant x \leqslant L$ in a reference configuration and whose mass density in that

configuration is ρ. The bar is placed between and in contact with two electrode plates of a condenser that is connected to a cell that provides electromotive force; see Fig. 1.

The applied electric field $e(t)$ and the temperature $\theta_0(t)$ of the environment surrounding the bar are prescribed. Initially, the bar is at the same temperature as the environment. Thus,

$$\theta(x,0) = \theta_0(0). \tag{2.1}$$

As the bar is composed of a ferroelectric crystal whose polar axis is normal to the electrodes, it is polarized either parallel or antiparallel to the electric field. Therefore, a thermoelectric process of the bar is characterized by the polarization intensity field $p(x,t)$ and the temperature field $\theta(x,t)$ where x denotes the location of a particle in the reference configuration and t is time.

In this study, the ferroelectric crystal is modeled as a thermopolarizable solid, which is characterized by its Helmholtz free-energy potential per unit mass $\psi(p,\theta)$. For such a material, the electric field e and entropy per unit mass η at a particle are related to p and θ by the constitutive relations

$$e = e(p,\theta) = \rho\psi_p(p,\theta), \qquad \eta = \eta(p,\theta) = -\psi_\theta(p,\theta). \tag{2.2}$$

In the next section, we shall write down the particular form of ψ, which may exist in one of multiple phases for suitable values of electric field and temperature.

At each instant t during a thermoelectrical process, the polarization intensity $p(x,t)$ and temperature gradient $\theta_x(x,t)$ vary smoothly within the bar except at domain boundaries; across a domain boundary, they suffer jump discontinuities. The electric field is constant along the bar and the temperature field is assumed to remain continuous throughout the bar. Away from a domain boundary, the first and second laws of thermodynamics require that

$$-q_x + \rho r = \rho\theta\eta_t, \qquad q\theta_x \leqslant 0, \tag{2.3}$$

respectively, where $q(x,t)$ is the heat flux in the $+x$-direction and $r(x,t)$ is the heat supply rate (to the bar) per unit mass. At a domain boundary $x = s(t)$, one has the associated jump conditions

$$q^+ - q^- = f\dot{s} + \rho\theta(\eta^+ - \eta^-)\dot{s}, \quad f\dot{s} \geqslant 0, \tag{2.4a,b}$$

where f is the driving traction or driving force acting on the domain boundary, which is defined by

$$f = \rho(\psi^+ - \psi^-) - e(p^+ - p^-). \tag{2.5}$$

In Eqs. (2.4a,b) and (2.5), we have written $h^\pm = h^\pm(t) = h(s(t)^\pm, t)$ for the limiting values of a field $h(x,t)$ as the domain boundary $x = s(t)$ is approached from either side. In order to interpret the driving traction from the energy point of view, we introduce the potential energy per unit reference volume $G(p;\theta,e)$ of the material:

$$G(p;\theta,e) = \rho\psi(p,\theta) - ep. \tag{2.6}$$

The value of the potential energy at an extremum of $G(\cdot;\theta,e)$ coincides with the Gibbs free energy per unit reference volume

$$g(p,\theta) = \rho\psi(p,\theta) - \rho\psi_p(p,\theta)p. \tag{2.7}$$

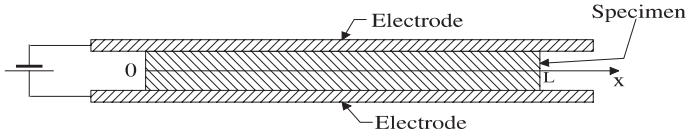

Fig. 1. The ferroelectric specimen placed between two electrode plates of a condenser connected to a cell of electromotive force.

In the present setting, the driving traction also equals the jump in Gibbs free energy across the domain boundary: $f = g^+ - g^-$.

In addition to the constitutive relations (2.2), we also have a heat conduction law

$$q = -k(p,\theta)\theta_x, \tag{2.8}$$

and a kinetic law

$$\dot{s} = V(f,\theta), \tag{2.9}$$

the former governs the flux of heat at points away from a domain boundary, while the latter controls the motion of a domain boundary. The heat conductivity k and the kinetic response function V are characteristic of the material.

In this paper, we consider a thermoelectrical process during which the bar involves only a single phase of the material for some initial interval of time, and two distinct phases at subsequent times. The kinetic law (2.9) controls the evolution of an existing domain boundary and therefore is operational only once the bar is in two-phase states. The initial transition of the bar from a single-phase configuration to a two-phase configuration is controlled by a nucleation criterion. The particular nucleation criterion that we shall use in our calculations will be described in the next section.

Next, we turn to thermal boundary conditions at the ends of the bar, and to the heat supply term r. With regard to the former, we suppose the heat transfer between the bar and the surrounding medium through the end surfaces is governed by Newton's law of cooling, so that

$$k\theta_x(0,t) = \xi[\theta(0,t) - \theta_0(t)], \qquad k\theta_x(L,t) = -\xi[\theta(L,t) - \theta_0(t)], \tag{2.10}$$

where $\xi \geqslant 0$ is a constant and $\theta_0(t)$ is the temperature of the environment; the special cases $\xi = 0$ and $\xi = \infty$ correspond to the respective cases in which the ends of the bar are perfectly insulated and have a prescribed temperature $\theta_0(t)$.

The heat supply term r, in the present one-dimensional study, represents the heat transfer across the lateral surface of the bar. We shall take this too to be controlled by Newton's law of cooling:

$$r(x,t) = -\zeta[\theta(x,t) - \theta_0(t)], \tag{2.11}$$

where $\zeta > 0$ is a constant.

Finally, we introduce the electric displacement defined by

$$d(x,t) = \varepsilon_0 e(x,t) + p(x,t), \tag{2.12}$$

where ε_0 is the permittivity of free space.

3. Constitutive model

We now describe the particular constitutive model that we shall use in our detailed calculations. This model was designed to be as simple as possible, while at the same time explicitly building upon the fact that the essential underlying mechanism is the transition of the material from one energy-well to another. The model incorporates the multiple-well structure of the free-energy function and includes an explicit kinetic rule based on the notion of thermal activation, as well as a nucleation criterion depending on the value of critical energy barrier. Even though here we introduce a three-well energy function, we restrict our attention to the two variants of ferroelectric phase at low temperatures.

3.1. Helmholtz free-energy

In this study, we use the Helmholtz free energy function constructed by Kim (2000) for our calculations. The expression for ψ is given sectionally on the (p,θ)-plane shown in Fig. 2, where the regions D_1, D_2 and D_3 are identified with the three phases of the material P, F^+ and F^-, respectively. The temperature levels θ_m and θ_M denote two critical values of temperature: for $\theta > \theta_M$ the material exists only in its paraelectric form, whereas for $\theta < \theta_m$ the material exists only in its ferroelectric forms.

In this paper, we will focus only on the range of temperature less than θ_m, but we describe the complete energy function, which is valid on the temperatures below θ_M and which includes the equation for the high temperature paraelectric phase. Then,

$$\rho\psi(p,\theta) = \begin{cases} (\chi/2)p^2 + \rho c\theta(1-\log(\theta/\theta_T)) & \text{on } D_1, \\ (\chi/2)(p-p_T)^2 + \chi\beta(p-p_T)(\theta-\theta_T) + \rho c\theta(1-\log(\theta/\theta_T)) - \rho\lambda_T(1-\theta/\theta_T) & \text{on } D_2, \\ (\chi/2)(p+p_T)^2 - \chi\beta(p+p_T)(\theta-\theta_T) + \rho c\theta(1-\log(\theta/\theta_T)) - \rho\lambda_T(1-\theta/\theta_T) & \text{on } D_3. \end{cases} \tag{3.1}$$

At each temperature below θ_M, the Helmholtz free-energy function is a piecewise quadratic function of polarization intensity that is convex on D_1, D_2 and D_3 and concave on the remaining unshaded portion of the (p,θ)-plane. At fixed temperatures between θ_m and θ_M, it is a three-well potential, with the local minima occurring at the smallest, intermediate and largest values of polarization intensity corresponding to F^-, P and F^+, respectively, whereas at a temperature below θ_m, it is a two-well potential corresponding to $F^+$and F^-. At the temperature θ_T, the three local minima have the same height and so the three phases F^+, F^- and P have the same value of Gibbs free energy. Thus, the material parameter θ_T represents the *transformation temperature*. The values of ψ at the two ferroelectric energy-wells coincide at every θ at which these energy-wells exist. For $\theta > \theta_T$, the ferroelectric wells are higher than the paraelectric well, while for $\theta < \theta_T$ they are lower, so that paraelectric is favorable at higher temperatures, ferroelectric at lower temperatures. It can be shown that the material parameter λ_T represents the *latent heat* of the paraelectric $\rightarrow$ ferroelectric transitions at the transformation temperature.

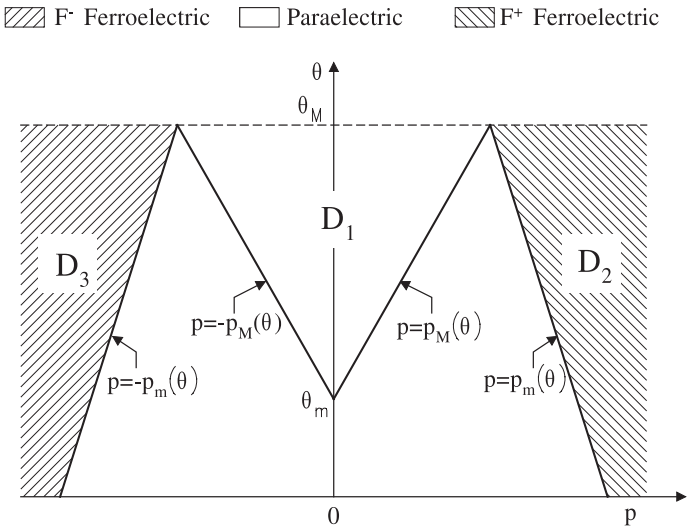

Fig. 2. Regions D_1, D_2, and D_3 in the (p,θ)-plane.

Therefore, the material at hand is characterized by the same *inverse susceptibility* at constant temperature χ and *specific heat* at constant polarization c of the phases; the *pyroelectric coefficients* 0, $-\beta$ and β of the respective phases P, F^+ and F^-; the electric field-free transformation temperature θ_T; the mass density ρ in the reference state; the latent heat λ_T at $\theta = \theta_T$ and the *transformation polarization intensity* p_T. A detailed discussion of the construction of this and a related potential as well as a description of their response during isothermal processes may be found in Kim (2000).

The electric field e and entropy η at a particle are related to p and θ by the constitutive relations $e = \rho\psi_p(p,\theta)$ and $\eta = -\psi_\theta(p,\theta)$. The electric field-response function is therefore given by

$$e(p,\theta) = \begin{cases} \chi p & \text{on } D_1, \\ \chi(p - p_T) + \chi\beta(\theta - \theta_T) & \text{on } D_2, \\ \chi(p + p_T) - \chi\beta(\theta - \theta_T) & \text{on } D_3. \end{cases} \tag{3.2}$$

In this paper, we are interested in the effects of the heat generated from a moving domain boundary during $F^+ \leftrightarrow F^-$ polarization reversals and so from now on, we pay attention only to those transformations. Consider a domain boundary located at $x = s(t)$ and suppose that the material on its left is in the F^+ variant of ferroelectric and the material on its right is in the F^- variant of ferroelectric. Then, the driving traction on this domain boundary may be calculated from Eqs. (2.5), (3.1) and (3.2) to be

$$f = 2\{p_T - \beta(\theta - \theta_T)\}\, e. \tag{3.3}$$

In view of the dissipation inequality $f\dot{s} \geqslant 0$, it follows that this domain boundary cannot move to the left if $f > 0$ and that it cannot move to the right if $f < 0$. That is, the $F^+ \to F^-$ transition cannot occur if $f > 0$ and the $F^- \to F^+$ transition cannot occur if $f > 0$. Therefore, assuming $p_T - \beta(\theta - \theta_T) > 0$ in the range of temperature that we consider, we may say that

$$\begin{aligned} &F^+ \text{ is favored when } e > 0, \\ &F^- \text{ is favored when } e < 0. \end{aligned} \tag{3.4}$$

Turning next to the remaining constitutive characteristics of the material, we take the heat conductivity of both phases to be the same, and constant:

$$k(p,\theta) = k = \text{constant} \quad \text{on } D_2, D_3. \tag{3.5}$$

3.2. Nucleation criterion

If a particle always chooses the phase that is stable from all phases available to it, then the response of the particle as the electric field is varied is fully determined by Eq. (3.4). That is, the particle is in the ferroelectric F^+ variant for a positive electric field and it is in the F^- variant for a negative electric field. In solids, however, particles can often remain for long times in states that are merely metastable and the initiation of the transition from a metastable phase to a stable phase is controlled by nucleation criterion. Now, we derive a specific nucleation criterion that is based on the critical value of energy barriers. Abeyaratne and Knowles (1993) have derived a nucleation criterion for shape memory alloys based on the same assumption.

Fig. 3 shows a schematic graph of the potential energy function $G(p;\theta,e)$ plotted versus p for a fixed pair (θ,e) at which only the two ferroelectric variants co-exist. The quantity $b_{23}(\theta,e)$ indicated in Fig. 3 is the energy barrier to a transformation from phase F^+ to phase F^- and similarly $b_{32}(\theta,e)$ is that of a transformation from phase F^- to F^+. In order to calculate these energy barriers, we have to know the value of potential energy at the local maxima located between the two local minima. Considering that the paraelectric phase is unstable below the temperature θ_m and that the value of polarization intensity of the paraelectric phase lies between those of the two ferroelectric variants, we may conclude that the local

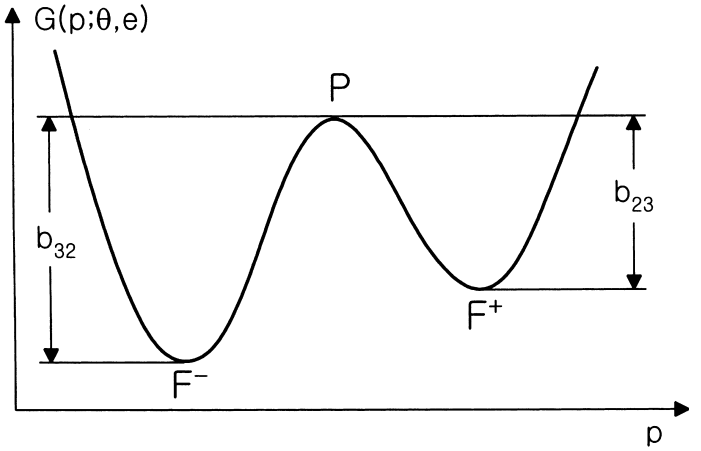

Fig. 3. Potential energy at a fixed temperature and electric field as a function of polarization intensity.

maxima corresponds to the paraelectric phase. Using Eq. (3.1) to calculate $G(p;\theta,e) = \rho\psi(p,\theta) - ep$ leads to the following expression for the energy barriers:

$$\begin{aligned} b_{23}(\theta,e) &= \{p_T - \beta(\theta-\theta_T)\}\ (e - e_0(\theta)),\\ b_{32}(\theta,e) &= -\{p_T - \beta(\theta-\theta_T)\}\ (e + e_0(\theta)), \end{aligned} \tag{3.6}$$

where the electric field $e_0(\theta)$ is the Maxwell electric field for the $P \leftrightarrow F^+$ transition given by

$$e_0(\theta)\{p_T - \beta(\theta-\theta_T)\} = \{\rho\lambda_T/\theta_T - (\chi\beta^2/2)(\theta-\theta_T)\}\ (\theta-\theta_T). \tag{3.7}$$

We suppose that a particle in the F^+ phase will transform to the F^- phase by nucleation if the relevant energy barrier $b_{23}(\theta,e)$ is less than some critical number N; the associated nucleation criterion is thus given by setting $b_{23}(\theta,e) = N$ in Eq. (3.6). In view of the symmetry of the potential energy function G, we assume that the critical energy barrier for the $F^- \to F^+$ transition is the same as that of the $F^+ \to F^-$ transition. Enforcing these restrictions and combining with Eq. (3.6) leads to the following nucleation criteria for the $F^+ \leftrightarrow F^-$ transitions:

$$e \leqslant e_0(\theta) + N/\{p_T - \beta(\theta-\theta_T)\} \quad \text{for } F^+ \to F^-, \tag{3.8a}$$

$$e \geqslant -e_0(\theta) - N/\{p_T - \beta(\theta-\theta_T)\} \quad \text{for } F^- \to F^+. \tag{3.8b}$$

Nucleation of the second phase will occur at the first instant during a thermoelectrical process at which Eq. (3.8a,b) is met at some particle in the bar. As the temperature field $\theta(x,t)$ is nonuniform in general, this will usually occur at some definite particle(s). However, noting that in an actual bar, imperfections would play an important role in determining the nucleation sites, we may take the nucleation sites arbitrarily. In this paper, we assume that the $F^- \to F^+$ transition would occur at $x = 0$ and the $F^+ \to F^-$ transition would commence at $x = L$.

3.3. Kinetic relation

The kinetic relation that is used for our calculations is developed based on the thermal activation theory. We follow the specific procedure taken by Abeyaratne and Knowles (1993) and Abeyaratne et al. (1994) to derive the kinetic law for shape memory alloys. As a domain boundary propagates through the bar, the

particle immediately in front of it 'jumps' from one local minimum of G to another, and an explicit model of the kinetic relation may be constructed by viewing this jumping process on a dipolar scale. The two local minima correspond to the equivalent configurations in which the elementary dipole is pointing in the $\pm$ direction of the ferroelectric axis. In order to jump from one minimum of G to the other, the dipole must acquire an energy at least as great as that represented by the relevant energy barrier: for a dipole undergoing $F^+ \to F^-$ transition this barrier is $b_{23}(\theta, e)$; for the $F^- \to F^+$ transition, it is $b_{32}(\theta, e)$. Under suitable assumptions about the statistics of this process, the probability that the energy of a dipole is at least as great as B is $\exp(-B/K\theta)$ where K is Boltzmann's constant. The average rate at which dipoles jump from one minimum to the other is taken to be proportional to the probability of exceeding the corresponding energy barrier; we assume for simplicity that the proportionality factor is the same for the $F^+ \to F^-$ and $F^- \to F^+$ transitions. The velocity $\dot{s}$ of the domain boundary, being the macroscopic measure of the net rate at which dipoles change from phase j to phase i, is then taken to be the difference in the average rates associated with the $i \to j$ and $j \to i$ transitions:

$$\dot{s} = R_{ij}\{\exp(-b_{ji}(\theta, e)/rK\theta) - \exp(-b_{ij}(\theta, e)/rK\theta)\}, \tag{3.9}$$

where r denotes the number of dipoles per unit reference volume and R_{ij} is a positive proportionality factor, related in part to the frequency with which dipoles attempt to cross over to the new phase.

Substituting Eq. (3.6) into Eq. (3.9) now leads to an explicit representation for the kinetic relations of the $F^+ \leftrightarrow F^-$ transitions in the form $\dot{s} = V(f, \theta)$:

$$\dot{s} = 2R\ \exp[\{\rho\lambda_T/\theta_T - (\chi\beta^2/2)(\theta - \theta_T)\}(\theta - \theta_T)/rK\theta] \sinh(f/2rK\theta), \tag{3.10}$$

where R is the proportionality constant between the two phases. These kinetic relations automatically satisfy the condition $f\dot{s} \geqslant 0$, so that any motion consistent with them will conform with the dissipation inequality (2.4b). According to Eq. (3.10), the function $V(f, \theta)$ increases monotonically with f, so that the greater the driving force, the faster the speed of domain boundary. If the driving force f is small, so that thermoelectrical processes take place close to phase equilibrium, then Eq. (3.10) can be approximated to give a linear kinetic relation:

$$\dot{s} \approx (R/rK\theta) \exp[\{\rho\lambda_T/\theta_T - (\chi\beta^2/2)(\theta - \theta_T)\}(\theta - \theta_T)/rK\theta]f. \tag{3.11}$$

4. Macroscopic thermo-electrical response

In this section, the basic equations of Section 2 is specialized to the particular material model described in Section 3. It follows from Eq. (3.2), that in each ferroelectric phase, the polarization intensity is related to the electric field and temperature by

$$\begin{aligned} p &= p_T + e/\chi - \beta(\theta - \theta_T) \quad \text{for } F^+ \text{ ferroelectric phase,} \\ p &= -p_T + e/\chi + \beta(\theta - \theta_T) \quad \text{for } F^- \text{ ferroelectric phase,} \end{aligned} \tag{4.1}$$

while the specific entropy is given, according to Eqs. (2.2), (3.1) and (4.1), by

$$\begin{aligned} \eta &= -\beta e/\rho + (\chi\beta^2/\rho)(\theta - \theta_T) + c\log(\theta/\theta_T) - \lambda_T/\theta_T \quad \text{for } F^+, \\ \eta &= \beta e/\rho + (\chi\beta^2/\rho)(\theta - \theta_T) + c\log(\theta/\theta_T) - \lambda_T/\theta_T \quad \text{for } F^-. \end{aligned} \tag{4.2}$$

In view of Eqs. (2.11) and (4.2), the energy equation (2.3) simplifies to

$$v\theta_{xx} = (1 + \beta g\theta)\theta_t - (g/\chi)\dot{e}\theta + (\zeta/c)(\theta - \theta_0) \quad \text{for } F^+, \tag{4.3a}$$

$$v\theta_{xx} = (1 + \beta g\theta)\theta_t + (g/\chi)\dot{e}\theta + (\zeta/c)(\theta - \theta_0) \quad \text{for } F^-, \tag{4.3b}$$

which must hold at every point in the respective part of the bar except at a domain boundary that may exist; here, v is the thermal diffusivity and g is a material constant, respectively, defined by

$$v = k/\rho c, \qquad g = \chi\beta/\rho c. \tag{4.4}$$

At a domain boundary, the jump condition (2.4a) must hold, which by Eqs. (2.8), (3.3), (3.5) and (4.2) can be written as

$$k(\theta_x^+ - \theta_x^-) = -2(p_T + \beta\theta_T)e\dot{s}, \tag{4.5}$$

where $\dot{s}$ is its propagation velocity. The kinetic law at a domain boundary requires that

$$\dot{s} = 2R\exp[\{\rho\lambda_T/\theta_T - (\chi\beta^2/2)(\theta-\theta_T)\}(\theta-\theta_T)/rK\theta]\ \sinh(f/2rK\theta),$$

$$\text{where}\quad f = 2\{p_T - \beta(\theta-\theta_T)\}e \tag{4.6}$$

and θ is the temperature at the domain boundary. Next, by integrating Eq. (4.1) with respect to x and dividing it by the length of the bar L, we get the average polarization intensity $p_a(t)$:

$$p_a(t) = p_T(2s(t)/L - 1) + e(t)/\chi + (\beta/L)\left[\int_{s(t)}^{L}(\theta(x,t)-\theta_T)\,dx - \int_0^{s(t)}(\theta(x,t)-\theta_T)\,dx\right]. \tag{4.7}$$

Finally, the average electric displacement $d_a(t)$ is, from Eqs. (2.12) and (4.7),

$$d_a(t) = \varepsilon_0 e(t) + p_a(t). \tag{4.8}$$

The nonlinear partial differential equations (4.3a,b) involve coupling between electrical and thermal effects. In the special case when the pyroelectric coefficients $\pm\beta$ vanish, it is linear and uncoupled from electrical effects. However, even in the case $\beta = 0$, the electrical and thermal effects are coupled through the jump condition (4.5), which involves both electric field and temperature. This jump condition represents a moving heat source whose magnitude and motion are not known a priori. The local heating at a domain boundary characterized by Eq. (4.5) arises in part due to the effect of latent heat and in part due to the effect of local energy dissipation; see Eq. (2.4b). It should be noted, however, that no local heating arises if the domain switching occurs under the condition of phase equilibrium, i.e., $f = 0$.

Now, we outline how these equations combine in order to characterize the thermoelectrical response of the bar. Suppose that initially, the entire bar is in the ferroelectric F^- phase, and the applied electric field intensity $e(t)$ and the environmental temperature $\theta_0(t)$ are prescribed. The bar will remain in F^- phase for some period of time $0 < t < t'$ during which the temperature $\theta(x,t)$ is governed by Eq. (4.3b), which now holds at every point in the bar, Eq. (4.7) with $s(t)$ set equal to zero, the initial condition (2.1), and the boundary conditions (2.10). At the instant t', according to the nucleation criterion Eq. (3.8b) and the discussion below it, a new domain boundary is nucleated at $x = 0$. In general circumstances, a number of domain boundaries may be generated depending on how many defects for nucleation exist. Such complexities cause no substantial differences and such a case can be treated in a manner entirely analogous to the simple case described above. Therefore, during the next stage, the bar consists of F^+ phase on $0 < x < s(t)$ and F^- phase on $s(t) < x < L$. During this stage, the location of the domain boundary $s(t)$, the temperature field $\theta(x,t)$ and the average polarization intensity $p_a(t)$ are controlled by Eqs. (4.3a,b) and (4.7), subject to the boundary conditions (2.10), the jump condition (4.5), the kinetic relation (4.6) and appropriate initial conditions. If at some later time the entire bar happens to be composed of F^+ ferroelectric, the reverse $F^+ \to F^-$ transition will occur when Eq. (3.8a) is satisfied.

Before solving the problem, it is convenient to nondimensionalize the equations by introducing the nondimensional variables:

$$x_* = x/L, \quad s_* = s/L, \quad t_* = tv/L^2, \quad \theta_* = \theta/\theta_T, \quad d_* = d/p_T,$$
$$e_* = e/\chi p_T, \quad f_* = f/\chi p_T^2, \quad p_{a*} = p_a/p_T, \quad p_* = p/p_T, \tag{4.9}$$

and the nondimensional parameters

$$\beta_* = \beta\theta_T/p_T, \quad \zeta_* = \zeta L^2/cv, \quad \theta_{0*} = \theta_0/\theta_T, \quad g_* = gp_T, \quad \xi_* = L\xi/\rho cv,$$
$$R_* = LR/v, \quad \lambda_{T*} = \rho\lambda_T/\chi p_T^2, \quad K_* = rK\theta_T/\chi p_T^2, \quad N_* = N/\chi p_T^2, \quad \varepsilon_{0*} = \chi\varepsilon_0. \tag{4.10}$$

Then, nondimensional kinetic relation is given by $V_*(f_*, \theta_*) = LV(f, \theta)/v$.

It is convenient to rewrite the governing mathematical problem in terms of these nondimensional variables. For simplicity, we shall omit the asterisks for Eqs. (4.11)–(4.17) shown below. Then, the respective equations (4.3a,b), (4.5), (4.6), (2.10), (4.7) and (4.8) can be rewritten as

$$\begin{aligned} &\theta_{xx} = (1 + \beta g\theta)\theta_t - g\dot{e}\theta + \zeta(\theta - \theta_0) \quad \text{for } 0 < x < s(t), \\ &\theta_{xx} = (1 + \beta g\theta)\theta_t + g\dot{e}\theta + \zeta(\theta - \theta_0) \quad \text{for } s(t) < x < 1, \end{aligned} \tag{4.11}$$

$$\theta_x^+ - \theta_x^- = -2(g/\beta)(1 + \beta)e\dot{s} \quad \text{for } x = s(t), \tag{4.12}$$

$$\begin{aligned} &\dot{s} = 2R \exp[\{\lambda_T - (\beta^2/2)(\theta - 1)\}(\theta - 1)/K\theta] \sinh(f/2K\theta), \\ &\text{where} \quad f = 2\{1 - \beta(\theta - 1)\}e, \end{aligned} \tag{4.13}$$

$$\theta_x = \xi(\theta - \theta_0) \quad \text{for } x = 0, \qquad \theta_x = -\xi(\theta - \theta_0) \quad \text{for } x = 1, \tag{4.14}$$

$$p_a(t) = (2s(t) - 1) + e(t) + \beta\left[\int_{s(t)}^{1} (\theta(x,t) - 1)\,dx - \int_0^{s(t)} (\theta(x,t) - 1)\,dx\right], \tag{4.15}$$

$$d_a(t) = \varepsilon_0 e(t) + p_a(t). \tag{4.16}$$

The respective nucleation criteria in Eq. (3.8) for the $F^+ \to F^-$ and the $F^- \to F^+$ transitions can be written as

$$\begin{aligned} &e \leqslant e_0(\theta) + N/\{1 - \beta(\theta - 1)\} \quad \text{for } F^+ \to F^-, \\ &e \geqslant -e_0(\theta) - N/\{1 - \beta(\theta - 1)\} \quad \text{for } F^- \to F^+. \end{aligned} \tag{4.17}$$

This "moving boundary problem" is similar to a classical Stefan problem but with two important differences: (i) here, the temperature of the moving interface $\theta(s(t), t)$ is not known in advance, and instead, the kinetic relation (4.13) is to be enforced, and (ii) the right-hand side of the energy jump condition (4.12) involves the electric field $e(t)$. We solved the problem at hand by using the finite difference method that was developed by Crank (1957) and then adapted by Kim and Abeyaratne (1995) to solve a moving boundary problem associated with a stress-induced phase transformation.

5. Results

In this section, we present the results of some specific calculations based on the model described in Section 4 and the finite difference algorithm used by Kim and Abeyaratne (1995). We will only describe the results associated with electrical loading, where the rate of electrical loading is prescribed and the environment temperature θ_0 is held constant. In fact, we shall always be concerned with a bar that is entirely in the F^- ferroelectric phase to start with, and we shall load and unload it electrically at constant loading-rates

$\pm(\mathrm{d}e/\mathrm{d}t)$. Thus, the sequence of events underlying all of the calculations to be described below are as follows: we consider a bar with ends satisfying thermal boundary conditions (2.10) that is initially entirely in the F^- ferroelectric phase. Its initial temperature is the same as that of the surrounding environment. The bar is subjected to a constant electrical loading rate $+(\mathrm{d}e/\mathrm{d}t)$. At some later instant, the nucleation criterion (3.8b) is satisfied and F^+ ferroelectric phase is nucleated at the left end of the bar. The F^+/F^- domain boundary emerges at this point and propagates to the right end of the bar. When it reaches the right end of the bar, the specimen is completely in the F^+ ferroelectric phase. Then, electrical unloading is carried out at the constant electrical loading rate $-(\mathrm{d}e/\mathrm{d}t)$. During this process, F^- ferroelectric phase is nucleated at the right end of the bar, and the F^+/F^- domain boundary moves toward the left end of the bar, transforming the specimen from the F^+ phase to the F^- phase. The temperature of the surrounding environment remains fixed at θ_0 throughout the process.

The values of the various nondimensional material parameters that we used in our calculations were as follows:

$$\begin{aligned} &\beta_* = 0.4094, \quad \zeta_* = 3.029, \quad \theta_{0*} = 0.583, \quad g_* = 6.058 \times 10^{-3}, \quad \xi_* = 9.253 \times 10^{-2}, \\ &R_* = 88014, \quad \lambda_{\mathrm{T}*} = 1.04 \times 10^{-3}, \quad K_* = 27.59, \quad N_* = 9.485 \times 10^{-3}, \quad \varepsilon_{0*} = 7.116 \times 10^{-4}. \end{aligned} \tag{5.1}$$

All of these values are of the correct order of magnitude for a $BaTiO_3$ ceramic except R_* and they are consistent with the values of the material parameters given in Kim (2000). The value of the mobility coefficient R_* was chosen arbitrarily so as to provide reasonable response curves.

Fig. 4 shows the temperature distribution along the bar at a fixed instant of time. The figure has been drawn at a particular instant during electrical loading at which the domain boundary is located at $x = L/2$. The three curves in the figure correspond to three different loading rates. It is seen that as the loading rate increases, so does the maximum temperature. Similar temperature distributions have been observed in the experiments done on shape memory alloys by Rodriguez and Brown (1975). At all the loading rates shown in the figure, the material behind the domain boundary is much hotter than the material ahead of it. This is because at the loading rates in the figure, there has not been sufficient time for the heat to diffuse along the bar. The fact that the temperature in the region ahead of the domain boundary is below the temperature of

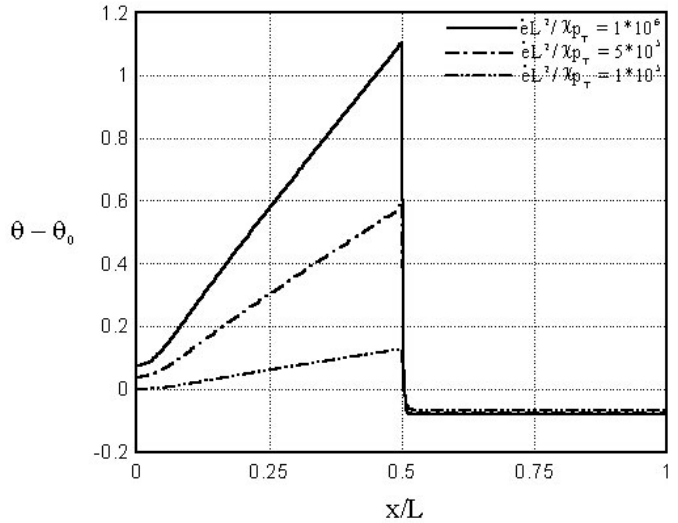

Fig. 4. Temperature distribution along the bar at the instant when $s = L/2$ for three different electrical loading rates.

the environment can be predicted from Eq. (4.3b), which governs the behavior of the bar consisting of only the F^- variant initially. At $t = 0$, the left-hand term and the third term in the right-hand side of Eq. (4.3b) vanish from the initial condition (2.1). Therefore, when the electrical loading rate (de/dt) is positive, θ_t should be negative and the temperature of the bar has to be decreased. We also carried out the calculations for electrical unloading and observed similar temperature distribution. That is, the temperature is higher in the region behind the domain boundary, while it is lower in the region ahead of the domain boundary.

Fig. 5 shows how the temperature at the domain boundary varies with its location during electrical loading. The three curves in the figure correspond to three different electrical loading rates. As expected, the temperature of domain boundary increases with the increase in the loading rate. At a given loading rate, the temperature of domain boundary increases as it moves toward the right end of the bar. Near the end, it tends to increase rapidly due to the thermal boundary condition at the right end of the bar. We also carried out calculations for the reverse $F^+ \rightarrow F^-$ transition and observed a similar increase in the temperature of domain boundary.

Fig. 6 shows the overall electric field-electric displacement response of the bar at three different electrical loading rates. We observe that the hysteresis loops rotate counterclockwise and increase in area as the loading rate increases. Similar behaviors have been observed for the isothermal responses of ferroelectric materials by Kim (1998, 2000). We also computed the isothermal responses of the model at which the temperature in the bar is always equal to the temperature of the environment, and compared them with the responses shown in Fig. 6. We found that the heights of hysteresis loops in isothermal responses are smaller, even though the difference is relatively small at the present loading rates, than those of hysteresis loops shown in Fig. 6. It is because the temperature of the bar is increased due to the heat generated from a moving domain boundary and according to the kinetic relation (3.10), the speed of domain boundary is decreased. The responses shown in the figure have been observed experimentally (e.g. Wieder, 1957; Campbell, 1957).

Fig. 7 shows how the average temperature of the bar increases with the number of cycles of applied field at three different electrical loading rates. The average temperature of the bar has been obtained by integrating the temperature with respect to x and dividing it by the length of the bar. In the figure, we observe

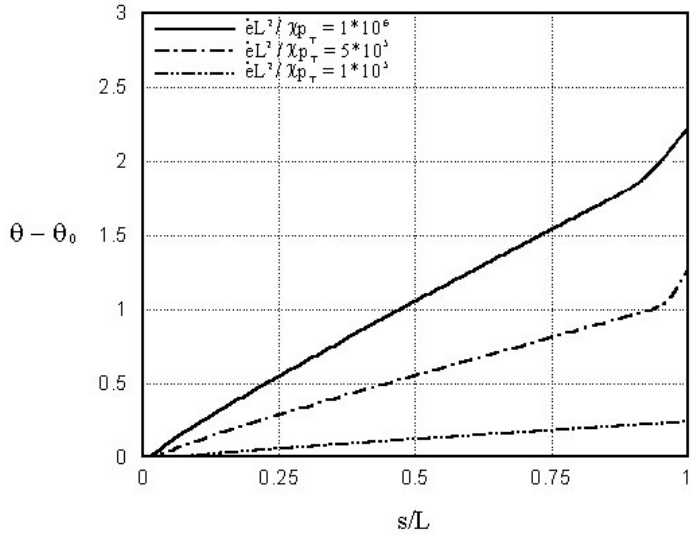

Fig. 5. Temperature at the domain boundary versus position of domain boundary for three different electrical loading rates.

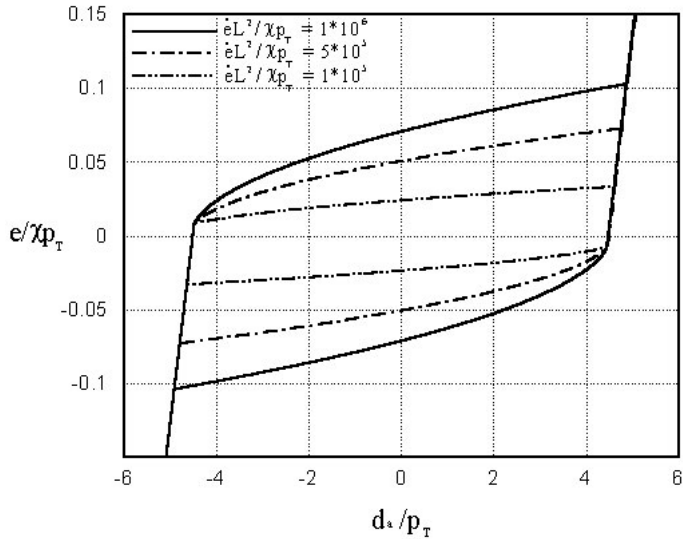

Fig. 6. Overall electric field-electric displacement curves of the bar for three different electrical loading rates.

that the average temperature increases rapidly during the initial loading cycles, but soon it approaches a steady state temperature as the number of cycles is increased. This may be explained as follows. Initially, the temperature difference between the bar and the environment is relatively small and the rate of heat transfer from the bar to the environment is smaller than that of heat generation inside the bar. This difference in the rate of heat transfer causes the initial rapid increase in the average temperature of the bar. As the temperature of the bar approaches the steady state temperature, the rate of heat transfer out of the bar is nearly in balance with the rate of heat generation in the bar and finally the bar is kept at a constant steady

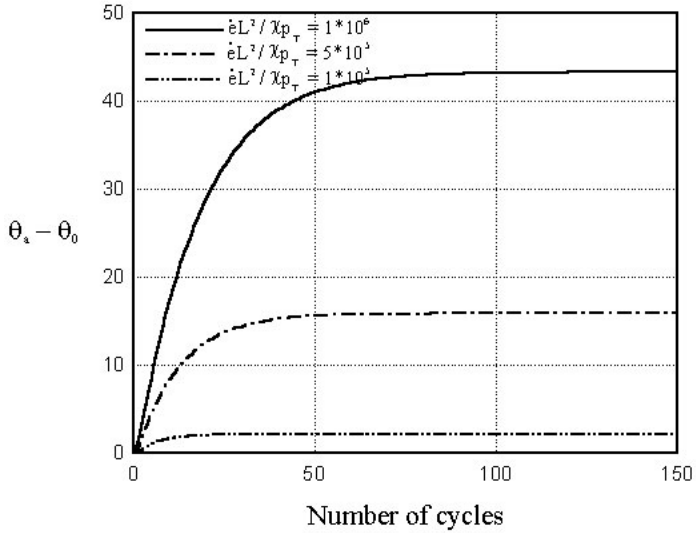

Fig. 7. Average temperature of the bar versus number of cycles of applied field for three different electrical loading rates.

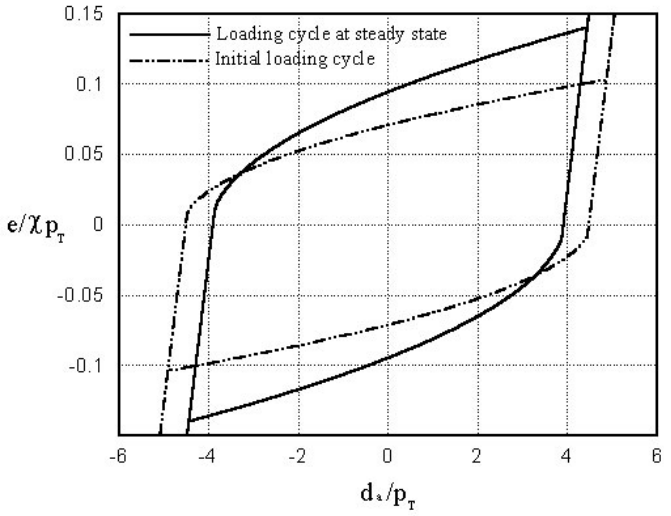

Fig. 8. Two electric field-electric displacement curves, one corresponding to initial loading cycle and the other corresponding to loading cycle at steady state.

state temperature. It is seen that the steady state temperature is higher at a faster loading rate. This is qualitatively in conformity with the experimental observations of Hill et al. (1996).

Fig. 8 compares two electric field-electric displacement responses at the fastest loading rate shown in Fig. 7: the solid one corresponds to initial loading cycle and the doted one to the loading cycle at steady state. That is, the former one is the response of the bar at the temperature of the environment 70°C and the latter one at the steady state temperature 113°C. It is seen that as the average temperature of the bar increases the width of hysteresis loops gets smaller due to the nonzero pyroelectric coefficient and the height of hysteresis loops gets bigger owing to the slower speed of domain boundary at the high steady state temperature.

Acknowledgements

The Korea Research Foundation has supported the research summarized here under grant number 1998-018-E00050.

References

Abeyaratne, R., Kim, S.J., Knowles, J.K., 1994. A one-dimensional continuum model for shape-memory alloys. Int. J. Solids Struct. 31, 2229–2249.

Abeyaratne, R., Knowles, J.K., 1993. A continuum model of a thermoelastic solid capable of undergoing phase transitions. J. Mech. Phys. Solids 41, 541–571.

Campbell, D.S., 1957. J. Electron. Control 3, 330.

Crank, J., 1957. Two methods for the numerical solution of moving boundary problems in diffusion and heat flow. Quart. J. Mech. Appl. Math. Part 2, 10, 220–231.

Ghandi, K., Hagwood, N.W., 1996. Nonlinear finite element modeling of phase transitions in electro-mechanically coupled material, 96 SPIE Proceedings, 2715, 121–139.

Hill, M.D., White, G.S., Hwang, C.S., Lloyd, I.K., 1996. Cyclic damage in lead zirconate titanate. J. Am. Ceram. Soc. 79, 1915–1920.

Hwang, S.C., Lynch, C.S., McMeeking, R.M., 1995. Ferroelectric/ferroelastic interactions and a polarization switching model. Acta Metall. Mater. 43, 2073–2084.

Jiang, Q., 1993. Macroscopic behavior of a bar undergoing the paraelectric–ferroelectric phase transformation. J. Mech. Phys. Solids 41, 1599–1635.

Jiang, Q., 1994. On the driving traction acting on a surface of discontinuity within a continuum in the presence of electromagnetic fields. J. Elasticity 34, 1–21.

Jona, F., Shirane, G., 1962. Ferroelectric Crystals. Pergamon Press, New York.

Kim, S.J., 1998. A simple continuum model for polarization reversals in ferroelectrics. Smart. Mater. Struct. 7, 572–579.

Kim, S.J., 2000. A one-dimensional continuum model for thermoelectric phase transformations in ferroelectrics. Int. J. Solids Struct. 37, 1145–1164.

Kim, S.J., Abeyaratne, R., 1995. On the effect of the heat generated during a stress-induced thermoelastic phase transformation. Cont. Mech. Thermo. 7, 311–332.

Rodriguez, C., Brown, L.C., 1975. The mechanical properties of some alloys. In: Perkins, J. (Ed.), Shape Memory Effects in Alloys, Plenum Press, New York, pp. 29–58.

Wieder, H.H., 1957. J. Appl. Phys. 28, 367.